

# Robust tracking control of an aircraft with critical actuator jam failures

Po-Chun Chan<sup>1</sup>  | Bor-Chin Chang<sup>2</sup>  | Mevlut Bayram<sup>2</sup> | Harry Kwatny<sup>2</sup> | Christine M. Belcastro<sup>3</sup>

<sup>1</sup>Department of Mechanical and Aerospace Engineering, National Defense University, Taoyuan City, Taiwan

<sup>2</sup>Department of Mechanical Engineering and Mechanics, Drexel University, Philadelphia, PA 1904, U.S.A

<sup>3</sup>Senior Researcher Engineer, NASA Langley Research Center, MS161, Hampton, VA, U.S.A

## Correspondence

Bor-Chin Chang, Department of Mechanical Engineering and Mechanics, Drexel University, Philadelphia, PA 19104, U.S.A.

Email: changbc@drexel.edu

## Funding information

Army Research Laboratory, Grant/Award Number: W911NF-15-2-0042

## Abstract

In this paper, we present a new single fixed controller approach based on the multivariable  $H_2$  control/regulator theory with internal model principle to solve a challenging control problem arising from an on-flight critical elevator jam at random positions that otherwise would need switching numerous controllers or online adaptive redesign approaches.

## KEYWORDS

actuator jam failures, aircraft flight control, robust tracking/regulation

## 1 | INTRODUCTION

### 1.1 | Motivation

Shortly after the Wright Brothers invented the airplane, Wilber Wright envisioned that the age of flying will have arrived when ‘this one feature (the ability to balance and steer)’ has been worked out [1]. Indeed, the age of flying certainly has arrived – civil air transportation has been our major means for distance travel, military aircraft have played significant roles in national defense, and the aviation industry has become an indispensable part of the world economy. There is no question that aircraft flight safety and efficiency are extremely important. There has been continuous effort by the aviation industry, NTSB, FAA, and NASA to reduce the aviation accident rate to a minimum. The improvement of aircraft design/maintenance, navigation/guidance equipment, traffic control systems, pilot training, and so on has

resulted in apparent decrease in the accident rate and fatalities in the past five decades, especially in civil transport – a record low accident rate of 0.151 per 100,000 flight hours in 2016 [2]. However, the GA (general aviation) fatal accident rate has remained relatively flat, which is still unacceptably high, with an accident rate around 5.9 per 100,000 flight hours, over the past ten years [2].

In the past 15 years, in-flight LOC (loss of control) has been the leading cause of aviation accidents, accounting for approximately 70 percent of all GA accident fatalities [3,4]. LOC events usually are highly complex, resulting from multiple adverse precursor conditions like subsystem/component failures, external hazards, human errors, and so on. The flight dynamics and behavior of the aircraft near or in the LOC regime [5–7] are very different from those inside the normal flight envelope, and are not well understood. Aircraft LOC recovery is an extremely challenging task for pilots. The reaction time for LOC recovery

usually is very limited, and pilots need to act quickly and correctly, to avoid escalating the crisis. In this paper, we will focus on addressing the issues arising from severe actuator jam failures in F/A-18 aircraft.

Elevator jam failure is the most serious actuator malfunction since it would cause a stall or a nose dive and only allow pilots a very small window of time to react and regain control of the aircraft. When an elevator jam occurs, it not only causes a loss of an important control authority but also creates a persistent disturbance against the aircraft. The loss of elevator control authority and the creation of the persistent disturbance would make it impossible for the aircraft to fly at the normal trim since the old equilibrium has disappeared. The disappearance of the normal equilibrium would cause flight mode confusion. If no appropriate action is taken in time, the aircraft would become unstable and uncontrollable.

Several control strategies have been proposed to deal with the issues arising from elevator jam, or in general, actuator jam failures. These strategies, to name a few, include mixer/pseudo-inverse [8–11], multivariable adaptive reconfiguration [12–17], multiple-model/switching [14], neural network based adaptive control [18], nonlinear inverse control [19–21], retrim/reoptimization control [22,23], servomechanism control [24–26], and so on.

## 1.2 | Full untrimmed nonlinear flight dynamics model is essential

Most existing control strategies for actuator jam failures utilize plant models trimmed at a fixed operating equilibrium of interest instead of considering the full untrimmed nonlinear aircraft flight dynamics model. In the following, we will demonstrate why the full untrimmed model is essential in the study of elevator jam issues. The full untrimmed nonlinear model is a global mathematical model of the real system, which can be trimmed at any operating equilibrium of interest to obtain a local trimmed model. A trim is a desired operating equilibrium. A trimmed model at a trim is a model described in terms of the coordinates with origin at this specific trim.

It is a common practice in aircraft flight control system design to design a specific controller for each trimmed model at every operating trim of interest. Due to the geometric symmetry of the aircraft structure, the flight dynamics system can be decoupled into two subsystems: one is the lateral system controlling the turns and lateral heading direction, and the other is the longitudinal system controlling the total air speed and the longitudinal flight path angle that dictates ascent, descent, or keeps a level flight. Since the elevator jam will not affect the lateral dynamics, we will mainly focus on the longitudinal subsystem.

The longitudinal flight dynamics system has four state variables and two control inputs as follows,

$$x = [V \ \alpha \ q \ \theta]^T, \quad u = [\delta_e \ \delta_T]^T \quad (1)$$

where  $V$ ,  $\alpha$ ,  $q$ ,  $\theta$ ,  $\delta_e$ , and  $\delta_T$  are the total speed, the angle of attack, the pitch rate, the pitch angle, the elevator control, and the thrust control, respectively.

If the lateral subsystem is set to fly straight without any roll or yaw motion, then for the F/A-18 aircraft to conduct a level flight with  $10^\circ$  angle of attack the longitudinal state vector and control input vector will be at the following trim,

*Trim N* :

$$\begin{aligned} \hat{x}_N &= [435.9\text{ft/s} \ 10^\circ \ 0^\circ/\text{s} \ 10^\circ]^T \\ \hat{u}_N &= [-1.26^\circ \ 5,470.5 \text{ lbf}]^T \end{aligned} \quad (2)$$

Note that the flight path angle  $\gamma = \theta - \alpha$  is zero, and both the angle of attack  $\alpha$  and the pitch angle  $\theta$  are  $10^\circ$ . The total air speed  $V$  is fixed at 435.9ft/s. A trimmed flight dynamics model at *TrimN* can be derived from the F/A-18 full untrimmed nonlinear flight dynamics model [27–29], and this trimmed model can be employed to design a controller to stabilize and improve the performance of the system at and around *TrimN*.

In case an elevator jam failure occurs and the jam position is at  $\delta_e = -10^\circ$ , the system not only loses 50% of its control authority, it will also be subject to a persistent aerodynamic disturbance caused by the jammed elevator control surface. This persistent disturbance would push the aircraft nose down. To offset the effect the thrust control  $\delta_T$  has to increase to pitch up the aircraft. Since *TrimN* has disappeared, it is impossible to recover the system back to the old trim. However, it is possible to recover the aircraft to another level flight trim, which is

*Trim Jn10* :

$$\begin{aligned} \hat{x}_{Jn10} &= [333.5\text{ft/s} \ 19.7^\circ \ 0^\circ/\text{s} \ 19.7^\circ]^T \\ \hat{u}_{Jn10} &= 10,771.6 \text{ lbf} \end{aligned} \quad (3)$$

This new level flight trim with  $19.7^\circ$  angle of attack is the only possible level flight trim the impaired aircraft can fly. The total air speed  $V$  is decreased from 435.9ft/s to 333.5ft/s and the thrust control input  $\delta_T$  is increased from 5470.5lbf to 10771.6lbf. The new trim *TrimJn10* is very different from the old trim *TrimN*.

The above discussions have revealed that the full untrimmed nonlinear flight dynamics model is essential not only in finding the operating equilibrium (the trim) of interest but also in assembling a linearized model at the trim so that a controller can be designed for each possible flight mode.

### 1.3 | Organization of the paper

The remainder of the paper is organized as follows. Section 2 demonstrates how an elevator jam will change the operating trim according to the jam position and explains the conventional approaches based on a fixed trim are inadequate in addressing the elevator jam issues. Possible remedies including the proposed solution are briefly described. In Section 3, we introduce the full untrimmed nonlinear F/A-18 flight dynamics model with actuator limits and dynamics constraints. The linearized model at particular trim condition will be explicitly described. Section 4 describes the structure of the nominal robust tracking controller that integrates the  $H_2$  optimal control theory, the multivariable servomechanism/regulator theory with internal model principle to achieve internal stability, robust altitude and flight path angle tracking, side-slip regulation, coordinated turn control, and so on. In Section 5, a single fixed contingency reconfigured controller is designed to address all the urgent issues caused by an elevator jam that may occur at any position from  $-23^\circ$  to  $+4^\circ$ . This reconfigured controller is able to automatically identify the new feasible level flight trim corresponding to the elevator jam position and stabilize the aircraft flight at the new trim. Furthermore, it is capable of conducting robust tracking of altitude, flight path angle, side-slip, and coordinated turn so that it can perform any required maneuvers to prepare for landing. In Section 6, simulations with the full untrimmed nonlinear F/A-18 model are presented to demonstrate the effectiveness of the proposed versatile robust tracking/regulation controller in mitigating the crisis caused by elevator jams. Section 7 is the conclusion. Section 8 provides a sketch proof of solution existence for two key equations employed in the design, and analysis of the closed-loop system stability after the trim has shifted to accommodate the elevator jam failures.

## 2 | ELEVATOR JAM ISSUES & POSSIBLE REMEDIES

In Section 1.2, we have used an F/A-18 longitudinal flight dynamics example to demonstrate that a fixed-trim linearized model is incapable of accurately describing the flight mode changes caused by elevator jam failures or assembling a linearized model for each trim (flight mode) of interest. On the other hand, with the full untrimmed nonlinear flight dynamics model we are able to find the new flight trim (flight mode) and assemble a linearized model for each trim of interest.

### 2.1 | Elevator jam issues

Assume the untrimmed nonlinear model is given as

$$\dot{x}(t) = f(x(t), u(t)) \quad (4)$$

where  $x(t)$  and  $u(t)$  are the state and control input vectors shown in Equation (1). Note that the equilibriums of the system are those  $(x, u)$  such that  $f(x, u) = 0$ . In addition to the natural origin equilibrium  $(0,0)$ , there exist infinite many equilibrium points on a two-dimensional equilibrium surface inside the 6-dimensional product space  $X \times U$ , where  $X$  is the 4-dimensional state space and  $U$  is the 2-dimensional control input space. This two-dimensional equilibrium surface is the operable regime of the aircraft.

Inside the operable regime, the total air speed  $V$  and the flight path angle  $\gamma = \alpha - \theta$  can be altered by varying the elevator and thrust controls  $\delta_e$  and  $\delta_T$ . If a level flight with  $10^\circ$  angle of attack is chosen, the desired operating equilibrium will be as shown in Equation (2) of Section 1.2.

If the elevator is jammed at  $\delta_e = \delta_{ej} = -10^\circ$ , the untrimmed nonlinear model of Equation (4) will become

$$\dot{x}(t) = f(x, \delta_T, \delta_{ej}) \quad (5)$$

Note that the jammed elevator control surface not only loses its control authority, it becomes a source of persistent disturbance. The only available control input is the thrust control  $\delta_T$ . Furthermore, the operable regime of the system has reduced to a one-dimensional equilibrium curve. If level flight requirement is added, the operable regime will further reduce to just one operating point, which is given by Equation (3) in Section 1.2.

If the elevator jam occurs at  $\delta_e = -20^\circ$ , the only level flight trim for the impaired aircraft will be

*Trim Jn20 :*

$$\begin{aligned} \hat{x}_{Jn20} &= [294.8 \text{ft/s } 27.5^\circ \ 0^\circ/\text{s } 27.5^\circ]^T \quad (6) \\ \hat{u}_{Jn20} &= 13,966.1 \text{ lbf} \end{aligned}$$

In case the elevator is jammed at  $\delta_e = 2^\circ$ , the only level flight trim for the impaired aircraft is

*Trim Jp2 :*

$$\begin{aligned} \hat{x}_{Jp2} &= [560.1 \text{ft/s } 5.47^\circ \ 0^\circ/\text{s } 5.47^\circ]^T \quad (7) \\ \hat{u}_{Jp2} &= 2,706.2 \text{ lbf} \end{aligned}$$

Note that there is only one level-flight trim associated with each elevator jam position, and these trims can be very different. For each trim, a trimmed dynamics model can be derived from the full untrimmed nonlinear

dynamics model. For instance, the linearized model at *TrimJn10* can be found as

$$\begin{aligned} \dot{\bar{x}}_{Jn10}(t) &= A_{10}\bar{x}_{Jn10}(t) + B_{10}\bar{u}_{Jn10}(t) \\ \bar{x}_{Jn10} &= [\bar{V} \quad \bar{\alpha} \quad \bar{q} \quad \bar{\theta}]^T, \quad \bar{u}_{Jn10} = \bar{\delta}_T \\ A_{10} &= \begin{bmatrix} -0.0588 & -21.272 & 0 & -32.2 \\ -0.0005 & -0.2 & 1 & 0 \\ 0 & -1.7533 & -0.2631 & 0 \\ 0 & 0 & 1 & 0 \end{bmatrix} \\ B_{10} &= [0.00091 \ 0 \ 0 \ 0]^T \end{aligned} \tag{8}$$

Based on this linearized model at *TrimJn10*, a state-feedback controller like the following

$$\begin{aligned} \bar{u}_{Jn10}(t) &= F_{10}\bar{x}_{Jn10}(t) \\ &= [-58.176 \ 4984.8 \ 1133.6 \ 4179.6] \bar{x}_{Jn10}(t) \end{aligned} \tag{9}$$

can be designed by the  $H_2$  optimization, the LQR approach, or simply pole-placement approach to stabilize and improve the performance of the system at and around *TrimJn10*.

### 2.2 | Possible remedies

A feedback connection of a trimmed controller with the full untrimmed nonlinear plant is shown in Figure 1. Note that the origins of  $(\bar{x}, \bar{u})$  and  $(x, u)$  are  $(\hat{x}, \hat{u})$  and  $(0,0)$ , respectively, and hence the offset adjustments  $\bar{x} = x - \hat{x}$  and  $u = \bar{u} - \hat{u}$  are required in the connection. For example, if the elevator jam failure occurs at  $\delta_e = -10^\circ$ , the feasible level flight trim:  $\hat{u} = 10, 771.6$ ,  $\hat{x} = \hat{x}_{Jn10}$ , and the controller  $F_k = F_{10}$  given by Equation (9) can be employed to conduct the simulation. It also can be seen from Equations (3), (6), (7), that as the elevator jam position varies, the feasible trim  $(\hat{x}, \hat{u})$  may change tremendously.

One of the biggest challenges caused by elevator jam failures is that the elevator jam position is not known *a priori* and when it occurs there is only very limited time to deal with the crisis before it becomes unmanageable. Since the feasible trim for the aircraft to fly after the jam is also unknown before the jam, it is impossible to predesign a

controller using a conventional approach to stabilize the system at an unknown trim. Therefore, possible solutions to address the elevator jam issues are limited to the following three categories. One is the multiple-model/switching category that predesigns multiple contingency controllers for the trims associated with all possible elevator jam positions. When an elevator jam is detected, one of the pre-designed controllers that is associated with the elevator jam position will be selected by the switching mechanism to serve as the contingency controller to address the elevator jam issue. These approaches are tedious and may require large amount of data space.

The second is the on-line design category, which includes the adaptive control and the retrim/reoptimization approaches. Since the dire situation caused by the elevator jam may worsen quickly, the computation needs to be much faster than the situation deterioration rate for the on-line design approaches to work. The third category is the servomechanism/regulator approach, in which the elevator jam position is considered as a constant disturbance, the magnitude of which is arbitrary and therefore the effect of the arbitrary constant disturbance can be regulated to zero at a steady state if a tracking/regulation control system is adequately designed. Our proposed remedy for the elevator jam failure is evolved from our early primitive works [24,26] in 2001 using the basic concept of servomechanism/regulator. Due to the inability to incorporate a trustworthy full untrimmed nonlinear flight dynamics model into the design process at that time, these early works only worked for minor elevator jam cases.

Our proposed remedy for the elevator jam failure is a single fixed predesigned versatile robust tracking/regulation contingency controller. The proposed approach does not require the knowledge of the new feasible trim. It only needs to know if the elevator is jammed and the approximate jam position. Upon the detection of an elevator jam, the contingency controller will replace the nominal controller and automatically lead the impaired aircraft to fly toward and eventually at the new feasible desired trim conformable to the new elevator jam condition. One may be wondering how can it be possible for the controller to lead the impaired aircraft to a feasible trim without knowing the trim beforehand. More apparently magical is that the controller is able to accomplish the mission without the knowledge of the dynamics model at the future feasible trim. In fact, the reasoning behind the magic is simple. It is simply a feedback with robust tracking/regulation. The controller just simply demands the impaired aircraft to fly according to a desired reference flight path angle. If the desired reference flight path angle is zero, the impaired aircraft will have no other choice but to go to the unique level flight trim.

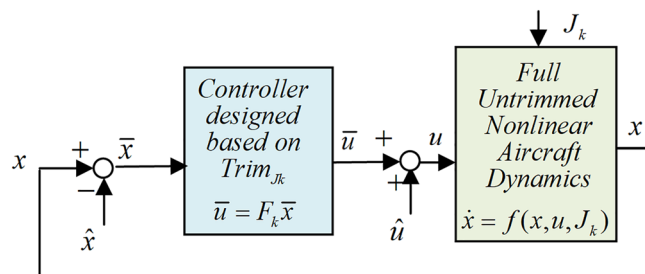


**FIGURE 1** Feedback connection of a trimmed controller with the full untrimmed plant [Color figure can be viewed at wileyonlinelibrary.com]

### 3 | NONLINEAR 6-DOF AIRCRAFT DYNAMICS MODEL

#### 3.1 | Equation of aircraft dynamics system

The test bed employed in this paper for the study of robust trajectory tracking under critical actuator jam failures is a six-DOF untrimmed 12-state nonlinear F/A-18 aircraft flight dynamics model. This model was originally created in FORTRAN by Buttrill et al. [27], then migrated to MATLAB by Chakraborty et al. to build a 9-state full nonlinear model in the study of ROA (region of attraction) of the vehicle [28]. Later this model was slightly modified by Chang et al. to construct a 6-DOF 12-state untrimmed nonlinear Simulink model in the study of aircraft trim recovery from highly nonlinear upset conditions [29].

The model is represented by the state equation,

$$\dot{x}(t) = f(x(t), u(t)) \quad (10a)$$

where the state vector is

$$x = [V \ \beta \ \alpha \ p \ q \ r \ \phi \ \theta \ \psi \ p_N \ p_E \ h]^T \quad (10b)$$

and the control input is

$$u = [\delta_a \ \delta_r \ \delta_e \ \delta_T]^T \quad (10c)$$

The 12 state variables are  $V$ : total speed (ft/s),  $\beta$ : side slip(rad),  $\alpha$ : angle of attack(rad),  $p$ : roll rate(rad/s),  $q$ : pitch rate(rad/s),  $r$ : yaw rate(rad/s),  $\phi$ : roll angle(rad),  $\theta$ : pitch angle(rad),  $\psi$ : yaw angle(rad),  $p_N$ : position north(ft),  $p_E$ : position east(ft),  $h$ : altitude(ft), and the 4 control inputs are  $\delta_a$ : aileron(rad),  $\delta_r$ : rudder(rad),  $\delta_e$ : elevator(rad),  $\delta_T$ : thrust(lbf). For computations the units of angles and angle rates have to be radians and radians/second, but for the ease of recognition by human they are displayed in degrees and degrees/second.

The 12 equations of motion inside Equation (10) are given in the following:

$$\begin{aligned} \dot{V} &= -\frac{1}{m}\bar{q}S(C_D\cos\beta - C_Y\sin\beta) + \frac{T}{m}\cos\alpha\cos\beta \\ &\quad + g(\sin\phi\cos\theta\sin\beta + \cos\phi\cos\theta\sin\alpha\cos\beta \\ &\quad - \sin\theta\cos\alpha\cos\beta) \\ \dot{\beta} &= -\frac{1}{mV}\bar{q}S(C_D\sin\beta + C_Y\cos\beta) + \frac{T}{mV}\cos\alpha\sin\beta \\ &\quad + p\sin\alpha - r\cos\alpha + \frac{g}{V}\cos\theta\sin\phi\cos\beta \\ &\quad + \frac{\sin\beta}{V}(g\cos\alpha\sin\theta - g\sin\alpha\cos\phi\cos\theta) \\ \dot{\alpha} &= -\frac{1}{mV\cos\beta}\bar{q}SC_L + q - \tan\beta(p\cos\alpha + r\sin\alpha) \\ &\quad + \frac{g}{V\cos\beta}(\cos\phi\cos\theta\cos\alpha + \sin\alpha\sin\theta) \\ &\quad - \frac{T\sin\alpha}{mV\cos\beta} \end{aligned} \quad (11a)$$

$$\begin{aligned} \dot{p} &= \{I_{zz}L + I_{xz}N - [I_{xz}(I_{yy} - I_{xx} - I_{zz})p + I_{xz}^2r \\ &\quad + I_{zz}(I_{zz} - I_{yy})r]q\}/(I_{xx}I_{zz} - I_{xz}^2) \end{aligned} \quad (11b)$$

$$\dot{q} = [M + (I_{zz} - I_{xx})pr + (r^2 - p^2)I_{xz}]/I_{yy}$$

$$\begin{aligned} \dot{r} &= \{I_{xz}L + I_{xx}N + [I_{xz}(I_{yy} - I_{xx} - I_{zz})r + I_{xz}^2p \\ &\quad + I_{xx}(I_{xx} - I_{yy})p]q\}/(I_{xx}I_{zz} - I_{xz}^2) \end{aligned}$$

$$\dot{\phi} = p + (q\sin\phi + r\cos\phi)\tan\theta$$

$$\dot{\theta} = q\cos\phi - r\sin\phi$$

$$\dot{\psi} = (q\sin\phi + r\cos\phi)\sec\theta \quad (11c)$$

$$\dot{p}_N = V\cos\beta\sin\alpha(\cos\phi\sin\theta\cos\psi + \sin\phi\sin\psi)$$

$$+ V\sin\beta(\sin\phi\sin\theta\cos\psi - \cos\phi\sin\psi)$$

$$+ V\cos\theta\cos\psi\cos\beta\cos\alpha$$

$$\dot{p}_E = V\cos\beta\sin\alpha(\cos\phi\sin\theta\sin\psi - \sin\phi\cos\psi)$$

$$+ V\sin\beta(\sin\phi\sin\theta\sin\psi + \cos\phi\cos\psi)$$

$$+ V\cos\theta\sin\psi\cos\beta\cos\alpha$$

$$\dot{h} = V\sin\theta\cos\beta\cos\alpha - V\cos\phi\cos\theta\cos\beta\sin\alpha$$

$$- V\sin\phi\cos\theta\sin\beta \quad (11d)$$

Note that the above 12 state equations are assembled in four groups: the translational velocity equations in Equation (11a), the angular velocity equations in Equation (11b), the Euler angle equations in Equation (11c), and translational position equations in Equation (11d). Due to page limitation, the moment and force equations, the aerodynamic coefficients, and the aircraft physical parameters required in the above equations of motion are not included; however, they can be found in [28].

#### 3.2 | Trim, equilibrium, and linearization

A common practice in the analysis and design of aircraft flight control systems is to determine a trim, which is loosely defined as a desired steady-state flight condition, so that the aircraft can safely fly at or in the vicinity of the trim. Although 'trim' seems to be a synonym of 'equilibrium', they actually are different. A trim is an equilibrium, but an equilibrium does not necessarily qualify to serve as a trim since not all equilibriums are desirable. In addition, a flight trim is only directly relevant to the four control inputs and the first eight state variables shown in Equation (10b). These eight trim-relevant state variables are the total speed  $V$ , the side slip  $\beta$ , the angle of attack  $\alpha$ , the roll rate  $p$ , the pitch rate  $q$ , the yaw rate  $r$ , the roll angle  $\phi$ , and the pitch angle  $\theta$ . The last four state variables of Equation (10b), that is, the yaw angle  $\psi$ , the position North and the position East variables  $p_N$  and  $p_E$ , and the altitude  $h$ , are irrelevant to the trimming process.

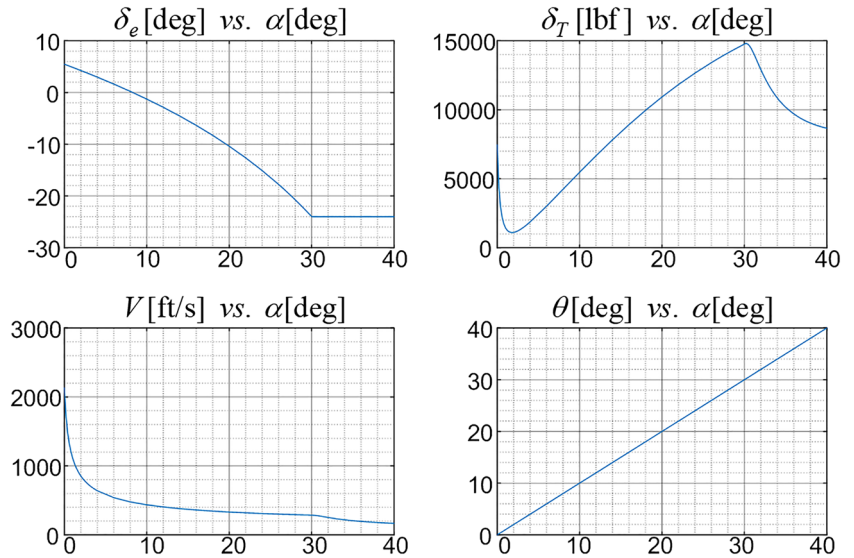


**FIGURE 2** Straight-level flight trim plot for F/A-18 model [Color figure can be viewed at wileyonlinelibrary.com]

Once a feasible trim is determined, the derivatives of the eight trim-relevant state variables should be zero at steady state, and the eight state variables and the control inputs should all approach constant values at steady state. Then these eight steady-state values together with the last four state equations in Equation (11) can be employed to compute the four trim-irrelevant state variables. Note that the derivatives of the four trim-irrelevant state variables are not required to be zero and they can continue to be functions of time when the other eight state variables and four control inputs all approach constant steady states.

Therefore, in the process of determining a trim or designing a stabilizing controller, we only need the following 8-state model:

$$\begin{aligned} \dot{x}(t) &= f(x(t), u(t)) \\ x &= [V \ \beta \ \alpha \ p \ q \ r \ \phi \ \theta]^T \\ u &= [\delta_a \ \delta_r \ \delta_e \ \delta_T]^T \end{aligned} \tag{12}$$

The control input constraints due to the magnitude and rate limitations are given as follows [27,28]:

$$\begin{aligned} -25^\circ < \delta_a < 25^\circ, & -30^\circ < \delta_r < 30^\circ, & -24^\circ < \delta_e < 10.5^\circ \\ 0\text{lb} < \delta_T < 20,000\text{lbf}, & -100^\circ/\text{s} < \dot{\delta}_a < 100^\circ/\text{s}, \\ -61^\circ/\text{s} < \dot{\delta}_r < 61^\circ/\text{s}, & -40^\circ/\text{s} < \dot{\delta}_e < 40^\circ/\text{s} \end{aligned} \tag{13}$$

Furthermore, the actuator dynamics bandwidths of  $\delta_a$ ,  $\delta_r$ ,  $\delta_e$ , and  $\delta_T$ , are described by  $48/(s + 48)$ ,  $40/(s + 40)$ ,  $30/(s + 30)$ , and  $30/(s + 30)$ , respectively.

Since an aircraft in general spends most of its flight time on straight level flight, which is also the most favorable flight trim to resume when aircraft is under stressful

condition, the nominal flight trim is chosen as the nominal trim  $Trim_N$  shown in the following.

$$\begin{aligned} \hat{x}_N &= [435.9\text{ft/s} \ 0^\circ \ 10^\circ \ 0^\circ/\text{s} \ 0^\circ/\text{s} \\ & \quad 0^\circ/\text{s} \ 0^\circ \ 10^\circ \ * \ * \ \text{ft} \ * \ \text{ft} \ * \ \text{ft}]^T \\ \hat{u}_N &= [0^\circ \ 0^\circ \ -1.26^\circ \ 5,470.5\text{lbf}] \end{aligned} \tag{14}$$

Note that the yaw angle and the three position state variables are left open (marked by \*) in  $Trim_N$  since they are not trim variables. It can be seen on the straight-level flight trim plot shown in Figure 2 that the total speed  $V$ , the thrust  $\delta_T$  and the elevator  $\delta_e$  are 435.9ft/s, 5,470.5lbf, and  $-1.26^\circ$ , respectively when both the angle of attack  $\alpha$  and the pitch angle  $\theta$  are equal to  $10^\circ$ . Meanwhile, the operating range of the elevator for straight-level flight is from  $5.4^\circ$  to  $-24^\circ$ , where the latter is due to the control surface swing limit in Equation (13) but the former is limited by the insufficient lift caused by too little angle of attack. In addition, there is a bifurcation point at  $\alpha = 1.5^\circ$  in the  $\delta_T$  vs.  $\alpha$  plot. If the angle of attack is less than  $1.5^\circ$ , the thrust would need to be increased tremendously to speed up and generate enough lift to maintain a level flight. We will utilize this plot later to explain the mitigable elevator jam range.

A common practice in aircraft flight control system design is to select a feasible flight trim, and design a linear or nonlinear controller so that the closed-loop system has desired performances at and around the trim. At the selected trim,  $Trim_N$ , we will first find the linearized model, analyze the open-loop system characteristics, and then design a control system to improve stability, enhance handling quality, and so on.

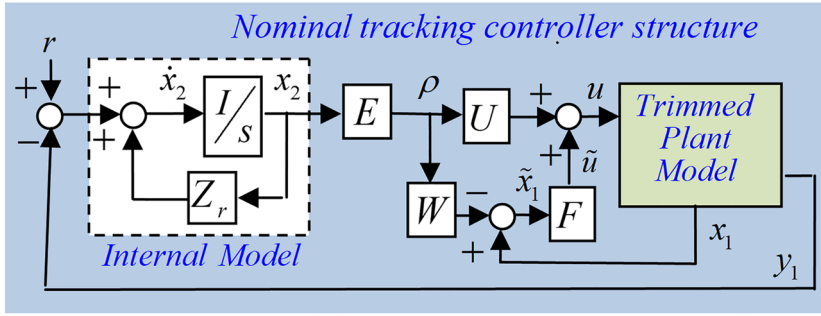


FIGURE 3 The basic structure of the nominal robust tracking controller [Color figure can be viewed at wileyonlinelibrary.com]

Due to the symmetrical structure of the aircraft, the 8-state linearized model can be further decoupled into two sets of 4-state models including the longitudinal dynamics equation:

$$\begin{aligned} \dot{\bar{x}}_{Lg}(t) &= A_{Lg}\bar{x}_{Lg}(t) + B_{Lg}\bar{u}_{Lg}(t) \\ \bar{x}_{Lg} &= [\bar{V} \quad \bar{\alpha} \quad \bar{q} \quad \bar{\theta}]^T, \quad \bar{u}_{Lg} = [\bar{\delta}_e \quad \bar{\delta}_r]^T \\ A_{Lg} &= \begin{bmatrix} -0.0239 & -28.3172 & 0 & -32.2 \\ -0.0003 & -0.3621 & 1 & 0 \\ 0 & -2.2115 & -0.2532 & 0 \\ 0 & 0 & 1 & 0 \end{bmatrix} \\ B_{Lg} &= \begin{bmatrix} -3.8114 & 0.001 \\ -0.0515 & 0 \\ -2.8791 & 0 \\ 0 & 0 \end{bmatrix} \end{aligned} \quad (15)$$

and the lateral dynamic equation:

$$\begin{aligned} \dot{\bar{x}}_{La}(t) &= A_{La}\bar{x}_{La}(t) + B_{La}\bar{u}_{La}(t) \\ \bar{x}_{La} &= [\bar{\beta} \quad \bar{p} \quad \bar{r} \quad \bar{\phi}]^T, \quad \bar{u}_{La} = [\bar{\delta}_a \quad \bar{\delta}_r]^T \\ A_{La} &= \begin{bmatrix} -0.0347 & 0.1736 & -0.9848 & 0.0727 \\ -8.543 & -0.8883 & 0.8762 & 0 \\ 0.886 & 0.0399 & -0.1895 & 0 \\ 0 & 1 & 0.1763 & 0 \end{bmatrix} \\ B_{La} &= \begin{bmatrix} -0.0149 & 0.0207 \\ 8.3321 & 0.9541 \\ -0.042 & -0.6277 \\ 0 & 0 \end{bmatrix} \end{aligned} \quad (16)$$

The eigenvalues associated with longitudinal model are at  $-0.3094 \pm j1.4800$ ,  $-0.0101 \pm j0.1010$  and the eigenvalues associated with the lateral model are  $-0.2870 \pm j1.4500$ ,  $-0.4890$ ,  $-0.0518$ . The trim is stable, but the open-loop characteristics are poor especially the phugoid mode with damping ratio  $\zeta = 0.1$  and natural frequency  $\omega_n = 0.102\text{rad/s}$  that would cause unacceptably long and large up and down oscillations in longitudinal motion. These issues can be easily fixed using feedback control.

## 4 | NOMINAL ROBUST TRACKING CONTROL

### 4.1 | Nominal tracking controller structure

The robust tracking controller structure shown in Figure 3 will be employed in the design of the longitudinal flight path tracking controller and the lateral coordinated turn controller. The trimmed plant model is described by

$$\begin{aligned} \dot{x}_1(t) &= Ax_1(t) + Bu(t), \quad y_1(t) = -C_1x_1(t) \\ e(t) &= r(t) - y_1(t) = D_{11}r(t) + C_1x_1(t) \end{aligned} \quad (17)$$

in which  $(A, B)$  can be  $(A_{Lg}, B_{Lg})$  of the longitudinal dynamics model of Equation (15) or  $(A_{La}, B_{La})$  of the lateral dynamics model of Equation (16), and the output vector  $y_1(t)$  consists of the variables to be tracked or regulated. One of the main objectives of the robust tracking control system is to make the regulated output follow the command, or the reference input  $r(t)$ , which is modeled as the output of the exogenous system,

$$\dot{r}(t) = Z_r r(t) \quad \text{with} \quad r(0) = r_0 \quad (18)$$

where  $Z_r$  has eigenvalues only on the imaginary axis of the complex plane and the initial exogenous state vector  $r_0$  is arbitrary. The most common exogenous signals include the step inputs with arbitrary magnitude and the sinusoidal signals with arbitrary amplitude and phase.

The internal model, which is a copy of the exogenous system dynamics in Equation (18) and the  $U$  and  $W$  matrices in the controller structure are employed to achieve zero tracking error at steady state, that is,  $y_1(\infty) = r(\infty)$ . The  $U$  and  $W$  matrices satisfying the following regulator equation [30–33]:

$$\begin{aligned} AW + BU - WZ_r &= 0 \\ C_1W + D_{11} &= 0 \end{aligned} \quad (19)$$

will transform the original coordinate  $(x_1, u)$  to the new one  $(\tilde{x}_1, \tilde{u})$ , where

$$\tilde{x}_1 = x_1 - W\rho, \quad \tilde{u} = u - U\rho \quad (20)$$

according to the vector  $\rho$ .

### 4.2 | Nominal tracking controller construction

The combination of the Internal Model and the Equilibrium-Shift regulation mechanism shown in Figure 3 is a perfect match that allows the former to automatically identify the correct vector value of  $\rho$  according to the plant variation so that the latter can complete the equilibrium shift and achieve robust tracking. In the following, we will describe how to find the matrices  $F$ ,  $U$ ,  $W$ , and  $E$  so that the closed-loop system is stable, the robust steady-state tracking is achieved, and the transient response is optimized subject to the actuator limitations and constraints shown in Equation (13).

#### 1) Construct The Augmented System

The first step is to combine the two subsystems, the trimmed plant model and internal model, into one augmented system with state vector  $x^T(t) = [x_1^T(t) \ x_2^T(t)]$ . The state equation for the augmented system will be

$$\dot{x}(t) = \begin{bmatrix} A & 0 \\ C_1 & Z_r \end{bmatrix} x(t) + \begin{bmatrix} 0 \\ D_{11} \end{bmatrix} r(t) + \begin{bmatrix} B \\ 0 \end{bmatrix} u(t) \quad (21)$$

#### 2) Optimize The Transient Response

Then the transient response optimization problem will be formulated as an  $H_2$  optimal control problem, which is to find a feedback control strategy

$$u(t) = F_1 x_1(t) + F_2 x_2(t) \quad (22)$$

so that the closed-loop system is internally stable and the following performance index integral is minimized.

$$\int_0^\infty (x^T(t)Qx(t) + u^T(t)Ru(t)) dt \quad (23)$$

where  $Q$  and  $R$  are positive semi-definite and positive definite, respectively. Note that the weighting matrices  $Q$  and  $R$  need to be chosen to optimize

the transient response while the actuator constraints shown in Equation (13) are not violated.

#### 3) Compute The Matrices $F$ , $U$ , $W$ , & $E$

Based on Equation (22), Equation (19), and the controller structure in Figure 3, the matrices  $F$ ,  $U$ ,  $W$  and  $E$  can be found by solving the following equations,

$$\begin{aligned} F &= F_1, & AW + BU - WZ_r &= 0 \\ C_1 W + D_{11} &= 0, & UE - F_1 WE - F_2 &= 0 \end{aligned} \quad (24)$$

### 4.3 | Nominal control of aircraft flight maneuvers

In addition to the straight level flight, the aircraft needs to be able to perform ascent, descent, and left or right coordinated turns. The structure of the nominal optimal robust tracking control system for aircraft flight maneuvers is shown in Figure 4. On the right and left of the figure, we can see the output  $u$  and the input  $y$  of the controller  $K_N$ , which respectively are connected to the full untrimmed nonlinear aircraft dynamics model shown in Figure 1. Since the controller is designed based on the linearized models at  $Trim_N$  of Equation (14), the designed control input  $\bar{u}(t)$  actually refers to  $\hat{u}_N$ , which means  $\bar{\delta}_T = 0\text{lb}$  is equivalent to  $\delta_T = 5,470.5\text{lb}$  and  $\bar{\delta}_e = 0^\circ$  is understood as  $\delta_e = -1.26^\circ$ . On the other hand, the data in the untrimmed output  $y(t)$  need to subtract the trim values before they enter the controller. For example,  $\bar{V} = V - 453.9\text{ft/s}$  and  $\bar{x}_{Lg} = x_{Lg} - [453.9\text{ft/s} \ 10^\circ \ 0^\circ/\text{s} \ 10^\circ]$ .

**Longitudinal Flight Path Tracking** The controller structure in Figure 4 is partitioned into two parts. The upper part is for the longitudinal stability, robustness, and flight path angle control. The flight path angle  $\gamma$  control is indirectly commanded by the altitude reference input  $h_{ref}$ . The flight path angle  $\gamma$  is a function of  $\alpha$ ,  $\theta$ ,  $\beta$ , and  $\phi$  as follows [34].

$$\begin{aligned} \sin \gamma &= -\cos \theta [\cos \beta \cos \phi \sin \alpha + \sin \beta \sin \phi] \\ &+ \cos \alpha \cos \beta \sin \theta \end{aligned} \quad (25)$$

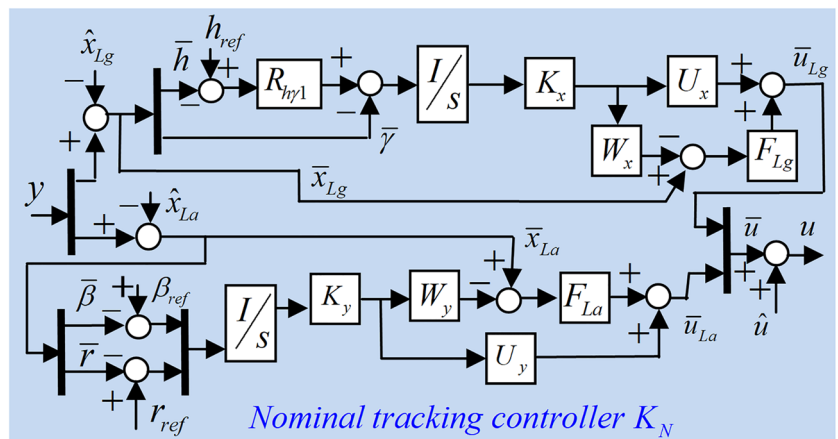


**FIGURE 4** Robust tracking control of nominal aircraft flight maneuvers [Color figure can be viewed at wileyonlinelibrary.com]



Note that for the straight level flight when  $\beta = 0^\circ$  and  $\phi = 0^\circ$ , this equation will reduce to  $\gamma = \theta - \alpha$ . The altitude  $\bar{h}$  is  $\bar{h} = h - h_{nom}$ , where  $h(t)$  is the real aircraft altitude and  $h_{nom}$  is the nominal altitude, assuming 25,000ft. Let the current aircraft altitude  $h$  be at the nominal value, 25,000ft, which means  $\bar{h}$  is zero. To increase the altitude to 30,000ft,  $h_{ref}$  should change from 0 to 5,000ft. Right after the  $h_{ref}$  change, the difference  $h_{ref} - \bar{h}$  will be 5,000, but it will decrease to zero as  $\bar{h}$  increases to 5,000ft (or  $h$  increases to the desired altitude 30,000ft). The change of altitude is carried out by controlling the flight path angle  $\bar{\gamma}$ , which is the real  $\gamma$  minus  $\gamma_N$ . The trimmed flight path angle usually is chosen to be 0. The  $h$  to  $\gamma$  scaler  $R_{h\gamma_1}$  is chosen to be  $0.003^\circ/\text{ft}$ .

The output of the  $R_{h\gamma_1}$  block, denoted as  $\gamma_{ref}$ , is employed as the reference input to the flight path angle tracking control subsystem, which consists of the internal model,  $I/s$  with  $Z_r = 0$ , the equilibrium-shift regulation matrices  $U_x$  and  $W_x$ , and the feedback control gain matrices  $F_{Lg}$  and  $E_x$ . These matrices can be found using the optimal nominal robust tracking controller design procedure shown in Section 4.2. The augmented system can be constructed as in Equation (21), where  $D_{11} = 1$ ,  $C_1 = [0 \ -1 \ 0 \ 1]$ ,  $A = A_{Lg}$ ,  $B = B_{Lg}$ , and  $Z_r = 0$ . The exogenous system matrix  $Z_r$  is chosen to be zero since the objective of the controller is to track the reference input, which is a step input function with arbitrary magnitude or a piecewise continuous function that can be approximated by a sequence of step functions. With this longitudinal augmented system, an optimal  $H_2$  feedback controller of the form in Equation (22) is obtained as  $F_x = [F_{1x} \ F_{2x}]$ , where

$$\begin{aligned} F_{1x} &= \begin{bmatrix} -0.097 & 0.315 & 1.619 & 3.309 \\ -65.68 & 10,432 & -67.52 & -10,300 \end{bmatrix} \\ F_{2x} &= \begin{bmatrix} -0.669 \\ 2,134 \end{bmatrix} \end{aligned} \quad (26)$$

Then by Equation (24), we can find the matrices of the longitudinal flight path tracking controller as follows.

$$\begin{aligned} F_{Lg} &= F_{1x}, \quad W_x = [-90.13 \ 0.0507 \ 0 \ 1.051]^T \\ U_x &= \begin{bmatrix} -0.0389 \\ 34,627 \end{bmatrix}, \quad E_x = 0.0547 \end{aligned} \quad (27)$$

Note that the poles of the closed-loop longitudinal tracking control system are  $-1.29 \pm j2.45$ ,  $-2.16$ ,  $-0.21$ , and  $-0.064$ .

### Lateral Coordinated Turn Control

The lower part of the controller structure in Figure 4 is for the lateral stability, robustness, and coordinated turn control. A coordinated turn can be manually achieved by coordinating the aileron and rudder controls to make a turn without causing a sideslip. The lateral tracking control subsystem shown in Figure 4 is designed to accomplish automatic coordinated turn control by regulating the two

lateral state variables, the yaw rate  $r(t)$  and the sideslip  $\beta(t)$ . Since  $\beta_N$  and  $r_N$  at *TrimN* are to be  $0^\circ$  and  $0^\circ/s$ , respectively, we have  $\bar{\beta}(t) = \beta(t)$  and  $\bar{r}(t) = r(t)$ . The sideslip reference input  $\beta_{ref}(t)$  is chosen to be the desired sideslip angle, which usually is  $0^\circ$ . The yaw rate reference input  $r_{ref}(t)$  is chosen to be the desired yaw rate, which can be determined by the desired turn angle (i.e., the yaw angle difference  $\Delta\psi$ ) or computed based on the turn rate  $\dot{\psi}$ . Note that the yaw rate  $r$  is not equal to  $\dot{\psi}$ .

The lateral sideslip and yaw rate tracking control subsystem consists of the internal model,  $I/s$  with  $Z_r = 0$ , the equilibrium-shift regulation matrices  $U_y$  and  $W_y$ , and the feedback control gain matrices  $F_{La}$  and  $E_y$ . These matrices can be found using the optimal nominal robust tracking controller design procedure shown in Section 4.2. The augmented system can be constructed as in Equation (21), where

$$\begin{aligned} C_1 &= \begin{bmatrix} 1 & 0 & 0 & 0 \\ 0 & 0 & 1 & 0 \end{bmatrix}, \quad D_{11} = \begin{bmatrix} -1 & 0 \\ 0 & -1 \end{bmatrix} \\ A &= A_{La}, \quad B = B_{La}, \quad Z_r = \begin{bmatrix} 0 & 0 \\ 0 & 0 \end{bmatrix} \end{aligned} \quad (28)$$

The exogenous system matrix  $Z_r$  is chosen to be a zero matrix for the same reason as described in the longitudinal case. A controller that can track the exogenous step inputs with arbitrary magnitude also can track well on any slowly varying reference signal. With the above lateral augmented system, an optimal LQR feedback controller of the form in Equation (22) is obtained as  $F_y = [F_{1y} \ F_{2y}]$ , where

$$\begin{aligned} F_{1y} &= \begin{bmatrix} 0.4805 & -0.9079 & -0.4385 & -0.327 \\ -2.924 & -0.6813 & 4.2146 & -0.2551 \end{bmatrix} \\ F_{2y} &= \begin{bmatrix} 0.0421 & 0.3134 \\ 0.9911 & -0.1331 \end{bmatrix} \end{aligned} \quad (29)$$

Then by Equation (24), we can find the matrices of the lateral sideslip and yaw rate tracking controller as follows.

$$\begin{aligned} F_{La} &= F_{1y}, \quad E_y = \begin{bmatrix} 0.2241 & -0.0142 \\ -0.0142 & 0.0671 \end{bmatrix} \\ W_y &= \begin{bmatrix} 1 & 0 \\ 0 & -0.176 \\ 0 & 1 \\ 0.3074 & 14.03 \end{bmatrix}, \quad U_y = \begin{bmatrix} 0.87 & -0.089 \\ 1.35 & -0.307 \end{bmatrix} \end{aligned} \quad (30)$$

Note that the poles of the closed-loop lateral tracking control system are  $-1.32 \pm j0.456$ ,  $-8.68$ ,  $-0.33$ ,  $-0.305$ , and  $-0.07$ .

## 5 | RECONFIGURED ROBUST TRACKING CONTROL

### 5.1 | Reconfigured tracking controller structure

The reconfigured tracking/regulation controller structure shown in Figure 5 will be employed in the design of a

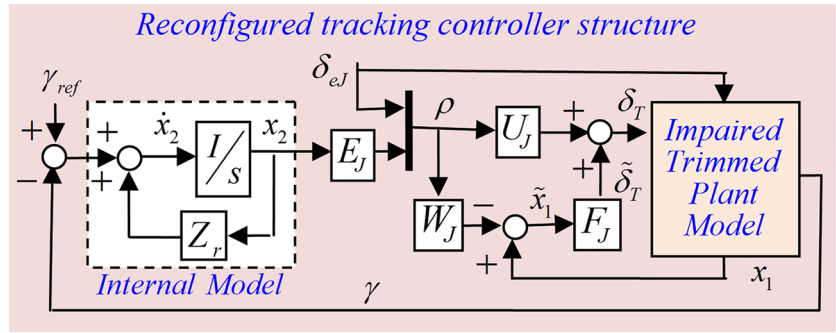


**FIGURE 5** The basic structure of the reconfigured robust tracking controller [Color figure can be viewed at wileyonlinelibrary.com]

reconfigured longitudinal tracking/regulation controller to address the issues caused by an elevator jam. The Impaired Trimmed Plant Model is described by

$$\begin{aligned} \dot{x}_1(t) &= Ax_1(t) + B_e \delta_{eJ}(t) + B_T \delta_T(t) \\ e(t) &= \gamma_{ref}(t) - \gamma(t) = D_{11} \gamma_{ref}(t) + C_1 x_1(t) \end{aligned} \quad (31)$$

where  $x_1(t) = x_{Lg}(t)$ ,  $A = A_{Lg}$ ,  $[B_e \ B_T] = B_{Lg}$ , and  $\gamma_{ref}(t)$  and  $\gamma(t)$  are the desired and the actual flight path angles, respectively. Note that the elevator control surface is jammed and no longer functioning as a control input; instead, it becomes the source of a persistent disturbance with arbitrary magnitude. The objective of the reconfigured longitudinal tracking/regulation control system is to stabilize the impaired system, minimize the effect of the aerodynamic force due to the jammed elevator, and ensure the aircraft's capability to perform the flight path angle tracking.

With the elevator jam, the longitudinal subsystem has lost the elevator control authority and become under-actuated with only the thrust control  $\delta_T$  remaining effective. On the other hand, the jammed elevator adds one more exogenous disturbance input  $\delta_{eJ}(t)$  to the system in addition to the reference input  $\gamma_{ref}(t)$ . These two exogenous inputs can be modeled as the output of the following exogenous system,

$$\begin{bmatrix} \dot{\delta}_{eJ}(t) \\ \dot{\gamma}_{ref}(t) \end{bmatrix} = \begin{bmatrix} Z_e & 0 \\ 0 & Z_r \end{bmatrix} \begin{bmatrix} \delta_{eJ}(t) \\ \gamma_{ref}(t) \end{bmatrix} \quad (32)$$

where  $Z_r$  and  $Z_e$  have eigenvalues only on the imaginary axis of the complex plane and the initial exogenous state vectors  $\delta_{eJ}(0)$  and  $\gamma_{ref}(0)$  are arbitrary. The most common exogenous signals include the step inputs with arbitrary magnitude and the sinusoidal signals with arbitrary amplitude and phase.

The internal model in Figure 5 is a copy of the exogenous system dynamics corresponding to  $Z_r$  in Equation (32). The internal model and the  $U_J$  and  $W_J$  matrices in the controller structure are employed to achieve zero tracking error and disturbance regulation at steady state, that is,  $\gamma(\infty) = \gamma_{ref}(\infty)$ . Let  $Z = \text{diag}(Z_e, Z_r)$ . Then the  $U_J$  and  $W_J$

matrices satisfying the following regulator equation:

$$\begin{aligned} AW_J + [B_e \ 0] + B_T U_J - W_J Z &= 0 \\ C_1 W_J + [0 \ D_{11}] &= 0 \end{aligned} \quad (33)$$

will transform the original coordinate  $(x_1, \delta_T)$  to the new one  $(\tilde{x}_1, \tilde{\delta}_T)$ , where

$$\tilde{x}_1 = x_1 - W_J \rho, \quad \tilde{\delta}_T = \delta_T - U_J \rho \quad (34)$$

according to value of the vector  $\rho$ .

## 5.2 | Reconfigured tracking controller design

The design of the reconfigured tracking controller is similar to that of the nominal tracking controller. The main difference is coming from the elevator jam. Now, there is only one control actuator, the thrust control  $\delta_T$ , available for longitudinal control. Furthermore, the reconfigured controller needs to address the persistent disturbance due to the aerodynamic force exerted on the jammed elevator surface. Note that the elevator jam position  $\delta_{eJ}$  information is fed back to the controller at  $\rho(1)$  so that the effect of the persistent disturbance can be mitigated.

In the following, we will describe how to find the matrices  $F_J$ ,  $U_J$ ,  $W_J$ , and  $E_J$  so that the closed-loop system is stable, the robust steady-state tracking is achieved, and the transient response is optimized subject to the actuator limitations and constraints shown in Equation (13).

### 1) Construct The Augmented System

The first step is to combine the two subsystems, the impaired trimmed plant model and internal model, into one augmented system with state vector  $x^T(t) = [x_1^T(t) \ x_2^T(t)]$ . The state equation for the augmented system will be

$$\dot{x}(t) = \begin{bmatrix} A & 0 \\ C_1 & Z \end{bmatrix} x(t) + \begin{bmatrix} B_e & 0 \\ 0 & D_{11} \end{bmatrix} \begin{bmatrix} \delta_{eJ}(t) \\ \gamma_{ref}(t) \end{bmatrix} + \begin{bmatrix} B_T \\ 0 \end{bmatrix} \delta_T(t) \quad (35)$$

## 2) Optimize The Transient Response

Then the transient response optimization problem will be formulated as an  $H_2$  optimal control problem, which is to find a feedback control strategy

$$\delta_T(t) = F_1 x_1(t) + F_2 x_2(t) \quad (36)$$

so that the closed-loop system is internally stable and the following performance index integral is minimized.

$$\int_0^{\infty} (x^T(t)Qx(t) + \delta_T^T(t)R\delta_T(t)) dt \quad (37)$$

where  $Q$  and  $R$  are positive semi-definite and positive definite, respectively. Note that the weighting matrices  $Q$  and  $R$  need to be chosen to optimize the transient response while the actuator constraints shown in Equation (13) are not violated.

## 3) Compute The Matrices $F_J$ , $U_J$ , $W_J$ , & $E_J$

Based on Equation (36), Equation (33), and the controller structure in Figure 5, the matrices  $F_J$ ,  $U_J$ ,  $W_J$  and  $E_J$  can be found by solving the following equations,

$$\begin{aligned} AW_J + [B_e \quad 0] + B_T U_J - W_J Z &= 0 \\ C_1 W_J + [0 \quad D_{11}] &= 0, \quad F_J = F_1 \\ U_{J2} E_J - F_1 W_{J2} E_J - F_2 &= 0 \end{aligned} \quad (38)$$

## 5.3 | Reconfigured control to address the issues arising from elevator jam failure

The reconfigured optimal robust tracking control system to address the issues arising from elevator jam is shown in Figure 6. Note that the nominal controller  $K_N$  shown in Figure 4 will become inadequate when an elevator jam failure occurs, since the jam will cause tremendous dynamics structure change in the longitudinal subsystem. A new controller needs to be specifically designed to address the three issues caused by the elevator jam: 1) the loss of elevator control authority, 2) the undesired persistent disturbance due to the aerodynamic force exerted on the jammed elevator surface, and 3) the disappearance of the nominal flight trim. We can see at the upper right

corner of Figure 6, there is only one control input, the thrust input  $\delta_T$ , available to control the longitudinal flight. Recall that  $u = \bar{u} + \hat{u}$ , where  $u$  is the real control input vector sent to the untrimmed nonlinear aircraft dynamics system, and  $\bar{u}$  is the output of the controller designed based on a trimmed dynamics model. A zero  $\bar{u}$  means that the real control input  $u$  is operating at its trimmed value,  $\hat{u} = \hat{u}_N$ .

The elevator jam position value  $\bar{\delta}_{eJ}$  shows up in two places – one is at the right side of the figure showing the real aircraft elevator is jammed at the position  $\bar{\delta}_{eJ} = \delta_{eJ} - 1.26^\circ$  and the other is on the top of the figure giving the jam position information to the reconfigured controller. The feedback loop in the reconfigured controller involves the internal model  $I/s$ , the regulator matrices  $U_J$ ,  $W_J$ , and the feedback gain matrices  $F_J$  and  $E_J$ . The internal model and the regulator matrices  $U_J$ ,  $W_J$  work together to guarantee robust steady-state tracking and regulation while the feedback gain matrices  $F_J$  and  $E_J$  can be designed to optimize the transient response and robust stability using the  $H_2$  or  $H_\infty$  control approaches.

As in the design of the nominal tracking controller, the altitude tracking control is accomplished via the control of the flight path angle. The output of the  $R_{\eta/2}$  block, denoted as  $\gamma_{ref}$ , is employed as the reference input to the flight path angle tracking control subsystem. The augmented system can be constructed as in Equation (35), where  $D_{11} = 1$ ,  $C_1 = [0 \ 1 \ 0 \ -1]$ ,  $A = A_{Lg}$ ,  $[B_e \ B_T] = B_{Lg}$  and  $Z_r = Z_e = 0$ . The exogenous system matrices  $Z_r$  and  $Z_e$  are chosen to be zero since both the reference input and the persistent disturbances are step input functions with arbitrary magnitude. With this augmented system, an  $H_2$  optimal feedback controller of the form in Equation (36) is obtained as  $F = [F_1 \ F_2]$ , where

$$\begin{aligned} F_1 &= [-67.81 \ 11,973 \ -133.3 \ -11,801] \\ F_2 &= 1,414.2 \end{aligned} \quad (39)$$

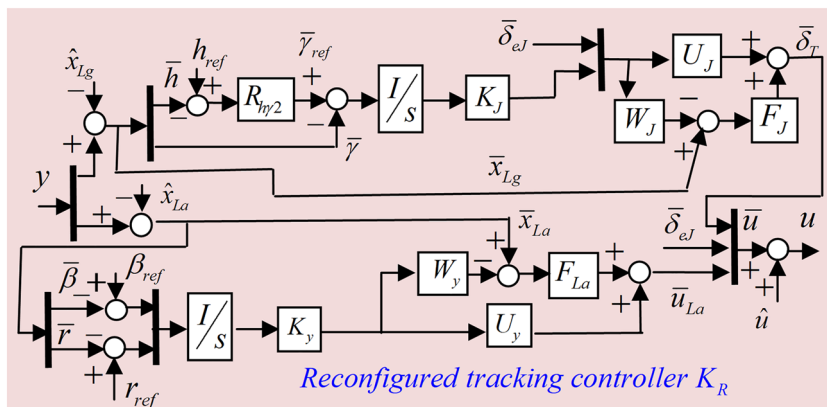


**FIGURE 6** Reconfigured tracking control of the impaired aircraft with elevator jam failures [Color figure can be viewed at [wileyonlinelibrary.com](http://wileyonlinelibrary.com)]

Then by Equation (38), we can find the matrices of the longitudinal reconfigured controller as follows.

$$U_J = \begin{bmatrix} -45,412 & 32,860 \end{bmatrix}, \quad F_J = F_1$$

$$W_J = \begin{bmatrix} 1,328.6 & -38.43 \\ -1.3019 & 0 \\ 0 & 0 \\ -1.3019 & 1 \end{bmatrix}, \quad E_J = 0.0336 \quad (40)$$

The poles of the closed-loop longitudinal control system are  $-0.309 \pm j1.48$ ,  $-0.026 \pm j0.105$ , and  $-0.038$ . Note that the lateral part of the reconfigured control system is the same as that in the nominal control system.

### 6 | SIMULATION

The results of 10 simulations will be presented in this section and displayed in Figures 7, 8, 9, 10, and 11, where each figure will consist of two simulations: one in solid

lines and the other in dotted lines. The solid-line will be referred to as the A(ascent)-simulations and dotted-line as the B(descent)-simulations. Therefore, the solid-line simulation on Figure 9 will be referred as Case 3A simulation. In all the simulations, the initial state is assumed at *TrimN*, which is a straight level flight with  $10^\circ$  angle of attack. The initial positions, altitude, and yaw angle are assumed at  $pN = 0\text{ft}$ ,  $pE = 0\text{ft}$ ,  $h = 25,000\text{ft}$ , and  $\psi = 0^\circ$ . For the first six cases, the aircraft is commanded to change altitude by ascending or descending 5,000ft at  $t = 0\text{s}$ , and then conduct a level coordinated turn at  $t = 200\text{s}$ . For Cases 4A, 4B, 5A and 5B, the aircraft is only commended to change altitude by ascending or descending 5,000ft at  $t = 0\text{s}$ , no coordinated turn will be performed.

Cases 1A and 1B show the performance of the nominal controller  $K_N$  with a healthy aircraft. Cases 2A and 2B demonstrate that the nominal controller  $K_N$  will become inadequate when a  $2.5^\circ$  elevator jam failure occurs. In

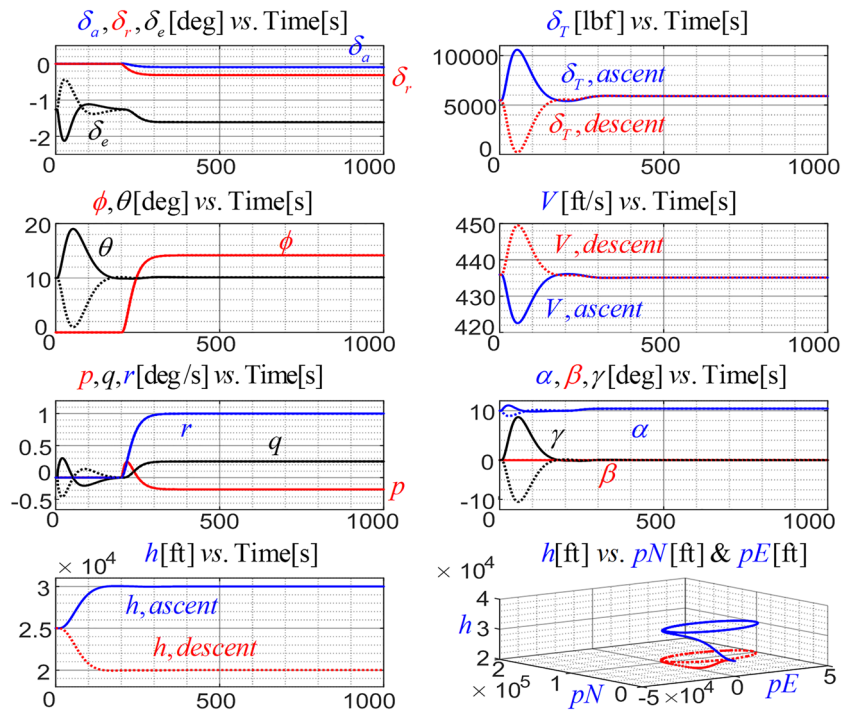


**FIGURE 7** Tracking performance of the nominal Controller  $K_N$  under normal flight conditions [Color figure can be viewed at wileyonlinelibrary.com]

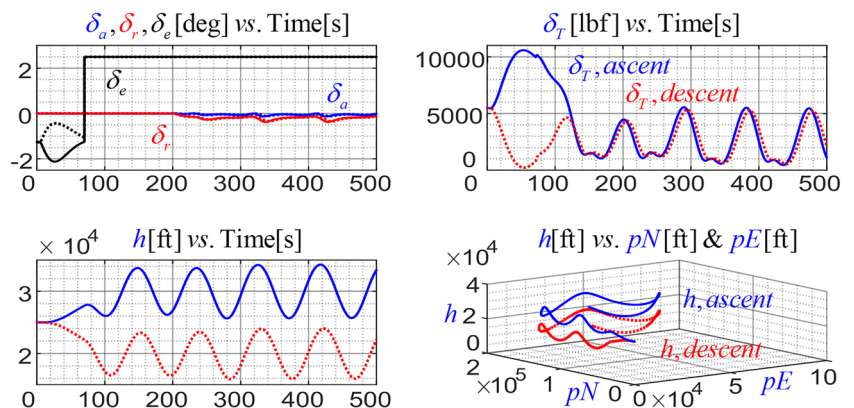


**FIGURE 8** The nominal Controller  $K_N$  becomes inadequate after the elevator jammed at  $\delta_e = 2.5^\circ$  [Color figure can be viewed at wileyonlinelibrary.com]

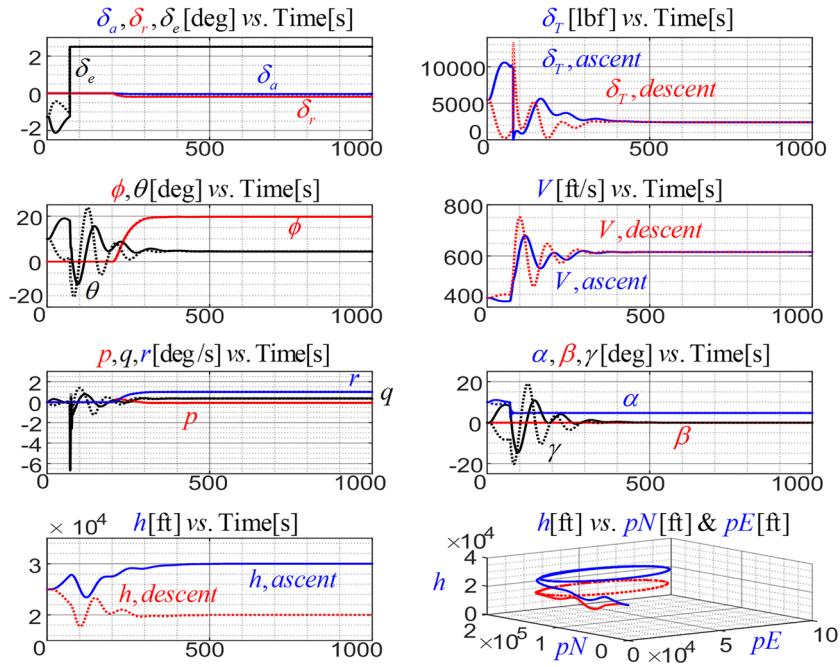


**FIGURE 9** Use the reconfigured controller  $K_R$  to mitigate the elevator jam failure at  $2.5^\circ$  [Color figure can be viewed at wileyonlinelibrary.com]

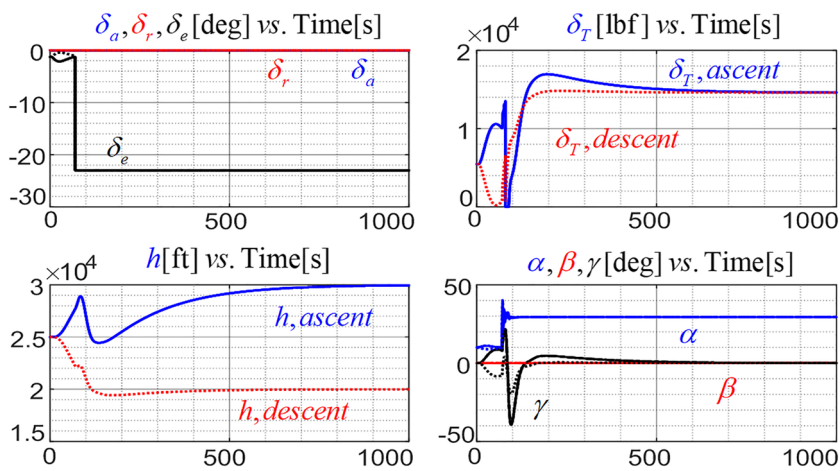


**FIGURE 10** Use the reconfigured controller  $K_R$  to mitigate the elevator jam failure at  $-23^\circ$  [Color figure can be viewed at wileyonlinelibrary.com]

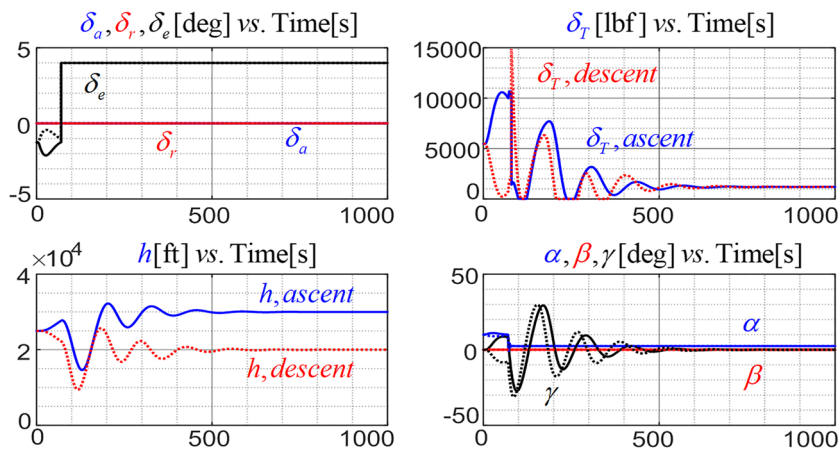


**FIGURE 11** Use the reconfigured controller  $K_R$  to mitigate the elevator jam at  $4^\circ$  [Color figure can be viewed at wileyonlinelibrary.com]

Cases 3A and 3B, we will see how well the contingency reconfigured controller  $K_R$  saves the aircraft from becoming loss of control. To further demonstrate the capability of

the reconfigured controller  $K_R$ , two extreme elevator jam positions at  $-23^\circ$  and  $+4^\circ$  are considered in Cases 4 and 5, respectively.

### 6.1 | $K_N$ for the healthy aircraft (Cases 1A & 1B)

The nominal controller  $K_N$  designed in Section 4 is employed in the Case 1A and 1B simulations, where the aircraft is assumed healthy without any actuator failures. The altitude tracking inputs  $h_{ref} = +5,000\text{ft}$  and  $h_{ref} = -5,000\text{ft}$  are applied in Cases 1A and 1B at  $t = 0\text{s}$  to command the aircraft to ascend to 30,000ft and descend to 20,000ft, respectively. Meanwhile, the side-slip and the yaw rate reference inputs, are set at  $\beta_{ref} = 0^\circ$  and  $r_{ref} = 0^\circ/\text{s}$  to keep straight flight. It can be seen from Figure 7 that by  $t = 200\text{s}$ , the straight flight ascent and descent are completed and the aircraft has returned to its nominal trim,  $TrimN$ .

At  $t = 200\text{s}$ , the yaw rate reference input is changed to  $r_{ref} = 1^\circ/\text{s}$ , while keeping the rest the same, to conduct a level coordinated turn. The graphs in Figure 7 show that at  $t = 400\text{s}$ , the coordinated turn has almost reached the steady-state and both of 1A and 1B graphs converge to the same equilibrium except for the altitude. The steady-state values  $x$ ,  $u$ ,  $\gamma$  and  $\dot{\psi}$  at  $t = 1,000\text{s}$  are given as follows. The two coordinated turn equilibriums of Case 1A and Case 1B are identical. The yaw angle turn rate is  $\dot{\psi} = \frac{\sin\phi}{\cos\theta}q + \frac{\cos\phi}{\cos\theta}r = 1.0476^\circ/\text{s}$ , which is different from the yaw rate  $r = 1^\circ/\text{s}$ . Note that the flight path angle formula  $\gamma = \theta - \alpha$  is only valid for straight flight; its general formula is given in Equation (25). With this formula, you will find

$$\begin{aligned} \sin\gamma &= -\cos\theta [\cos\beta \cos\phi \sin\alpha + \sin\beta \sin\phi] \\ &+ \cos\alpha \cos\beta \sin\theta = 0 \end{aligned}$$

which means  $\gamma = 0$  at the steady state.

$$\begin{aligned} x_{1A} &= [435.12\text{ft/s} \quad 0^\circ \quad 10.42^\circ \quad -0.18^\circ/\text{s} \\ &\quad 0.25^\circ/\text{s} \quad 1^\circ/\text{s} \quad 14.17^\circ \quad 10.11^\circ \\ &\quad *^\circ \quad * \text{ft} \quad * \text{ft} \quad 30,000\text{ft}]^T \end{aligned} \quad (41)$$

$$\begin{aligned} u_{1A} &= [-0.09^\circ \quad -0.31^\circ \quad -1.61^\circ \quad 5,898\text{lb}]^T \\ \gamma_{1A} &= 0^\circ, \quad \dot{\psi}_{1A} = 1.0476^\circ/\text{s} \end{aligned}$$

$$\begin{aligned} x_{1B} &= [435.12\text{ft/s} \quad 0^\circ \quad 10.42^\circ \quad -0.18^\circ/\text{s} \\ &\quad 0.25^\circ/\text{s} \quad 1^\circ/\text{s} \quad 14.17^\circ \quad 10.11^\circ \\ &\quad *^\circ \quad * \text{ft} \quad * \text{ft} \quad 20,000\text{ft}]^T \end{aligned} \quad (42)$$

$$\begin{aligned} u_{1B} &= [-0.09^\circ \quad -0.31^\circ \quad -1.61^\circ \quad 5,898\text{lb}]^T \\ \gamma_{1B} &= 0^\circ, \quad \dot{\psi}_{1B} = 1.0476^\circ/\text{s} \end{aligned}$$

### 6.2 | $K_N$ becomes inadequate after elevator jammed at $\delta_e = 2.5^\circ$ (Cases 2A & 2B)

In Cases 2A and 2B, elevator jams was assumed to occur at  $t = 70\text{s}$ , but no action was taken to mitigate the failure and the nominal controller  $K_N$ , now inadequate, still continued

its old control strategy without knowing the loss of the elevator control, the presence of the newly created persistent disturbance, and the disappearance of the nominal trim. It can be seen from the graphs in Figure 8 that the aircraft lost stability shortly after the elevator jam for both Cases 2A and 2B.

### 6.3 | $K_R$ to mitigate the elevator jam failure at $\delta_e = 2.5^\circ$ (Cases 3A & 3B)

The elevator jam occurred at  $t = 70\text{s}$ , but the reconfigured controller  $K_R$  did not engage until 10 seconds later. During this 10s period, the situation continued to deteriorate since the nominal controller  $K_N$  is unable to deal with the crisis. After  $K_R$  engaged at  $t = 80\text{s}$ , the situation started to get under control and by  $t = 400\text{s}$ , the system has almost reached the steady state of the coordinated turn and both graphs of Cases 3A and 3B are converging to the same equilibrium as shown in Figure 9. The steady-state values of  $x$ ,  $u$ ,  $\gamma$  and  $\dot{\psi}$  at  $t = 1,000\text{s}$  are given as follows. Note that the equilibriums of Cases 3A and 3B are identical, but they are different from the equilibriums of Cases 1A and 1B. The original nominal equilibriums have disappeared due to the elevator jam, but the controller  $K_R$  is able to identify the new feasible coordinated turn equilibrium and stabilize the system at the new equilibrium.

$$\begin{aligned} x_{3A} &= [615.41\text{ft/s} \quad 0^\circ \quad 4.7^\circ \quad -0.08^\circ/\text{s} \\ &\quad 0.36^\circ/\text{s} \quad 1^\circ/\text{s} \quad 19.71^\circ \quad 4.43^\circ \\ &\quad *^\circ \quad * \text{ft} \quad * \text{ft} \quad 30,000\text{ft}]^T \end{aligned} \quad (43)$$

$$\begin{aligned} u_{3A} &= [-0.04^\circ \quad -0.19^\circ \quad 2.5^\circ \quad 2,397.4\text{lb}]^T \\ \gamma_{3A} &= 0^\circ, \quad \dot{\psi}_{3A} = 1.0654^\circ/\text{s} \end{aligned}$$

$$\begin{aligned} x_{3B} &= [615.41\text{ft/s} \quad 0^\circ \quad 4.7^\circ \quad -0.08^\circ/\text{s} \\ &\quad 0.36^\circ/\text{s} \quad 1^\circ/\text{s} \quad 19.71^\circ \quad 4.43^\circ \\ &\quad *^\circ \quad * \text{ft} \quad * \text{ft} \quad 20,000\text{ft}]^T \end{aligned} \quad (44)$$

$$\begin{aligned} u_{3B} &= [-0.04^\circ \quad -0.19^\circ \quad 2.5^\circ \quad 2,397.4\text{lb}]^T \\ \gamma_{3B} &= 0^\circ, \quad \dot{\psi}_{3B} = 1.0654^\circ/\text{s} \end{aligned}$$

### 6.4 | $K_R$ to mitigate the elevator jam failure at $\delta_e = -23^\circ$ (Cases 4A & 4B)

In Cases 4A and 4B, the elevator jam occurs at  $t = 70\text{s}$  with the jam position at  $-23^\circ$ , which is close to the physical limit of the elevator control. As can be seen from Figure 10, almost immediately after the jam the angle of attack jumped from around  $10^\circ$  up to  $40^\circ$  causing the total speed to drop from 430ft/s to about 200ft/s. It was almost at a stall condition before the reconfigured controller  $K_R$  engaged at  $t = 80\text{s}$ . The controller  $K_R$ , with only the thrust control at its disposal, was able to neutralize the effect of the

persistent aerodynamic disturbance, prevent the aircraft from loss of control, identify a new feasible safe trim, and bring the aircraft to fly at the new safe trim.

$$\begin{aligned} x_{4A} &= [288.3\text{ft/s } 0^\circ \ 29.4^\circ \ 0^\circ/\text{s} \\ &\quad 0^\circ/\text{s } 0^\circ/\text{s } 0^\circ \ 29.4^\circ \\ &\quad *^\circ \ * \text{ft} \ * \text{ft} \ 30,000\text{ft}]^T \end{aligned} \quad (45)$$

$$\begin{aligned} u_{4A} &= [0^\circ \ 0^\circ \ -23^\circ \ 14, 586\text{lb}]^T \\ \gamma_{4A} &= 0^\circ, \quad \dot{\psi}_{4A} = 0^\circ/\text{s} \\ x_{4B} &= [288.3\text{ft/s } 0^\circ \ 29.4^\circ \ 0^\circ/\text{s} \\ &\quad 0^\circ/\text{s } 0^\circ/\text{s } 0^\circ \ 29.4^\circ \\ &\quad *^\circ \ * \text{ft} \ * \text{ft} \ 20,000\text{ft}]^T \end{aligned} \quad (46)$$

$$\begin{aligned} u_{4B} &= [0^\circ \ 0^\circ \ -23^\circ \ 14, 586\text{lb}]^T \\ \gamma_{4B} &= 0^\circ, \quad \dot{\psi}_{4B} = 0^\circ/\text{s} \end{aligned}$$

Note that the above straight level flight equilibrium is consistent with the straight-level flight trim curve shown in Figure 2. At this extreme elevator jam position ( $-23^\circ$ ), the aircraft does not have much option but to fly at a very high angle of attack with a very high thrust input.

### 6.5 | $K_R$ to mitigate elevator jam failure at $\delta_e = 4^\circ$ (Cases 5A & 5B)

In Cases 5A and 5B, the elevator jam occurs at  $t = 70\text{s}$  with another extreme jam position at  $4^\circ$ , which is close to the opposite end of the working range of the elevator control. As can be seen from Figure 11, almost immediately after the jam the angle of attack dropped from  $10^\circ$  down to  $2^\circ$  and the flight path angle changed from around  $10^\circ$  to about  $-30^\circ$  causing a tremendous loss of altitude. It was almost at a stall condition before the reconfigured controller  $K_R$  engaged at  $t = 80\text{s}$ . The controller  $K_R$ , with only the thrust control at its disposal, was able to neutralize the effect of the persistent aerodynamic disturbance, prevent the aircraft from loss of control, identify a new feasible safe trim, and bring the aircraft to fly at the new safe trim. This new trim is the steady-state equilibrium of the Case 5A and Case 5B flights shown as follows.

$$\begin{aligned} x_{5A} &= [789.87\text{ft/s } 0^\circ \ 2.41^\circ \ 0^\circ/\text{s} \\ &\quad 0^\circ/\text{s } 0^\circ/\text{s } 0^\circ \ 2.41^\circ \\ &\quad *^\circ \ * \text{ft} \ * \text{ft} \ 30,000\text{ft}]^T \end{aligned} \quad (47)$$

$$\begin{aligned} u_{5A} &= [0^\circ \ 0^\circ \ 4^\circ \ 1, 195.4\text{lb}]^T \\ \gamma_{5A} &= 0^\circ, \quad \dot{\psi}_{5A} = 0^\circ/\text{s} \\ x_{5B} &= [789.87\text{ft/s } 0^\circ \ 2.41^\circ \ 0^\circ/\text{s} \\ &\quad 0^\circ/\text{s } 0^\circ/\text{s } 0^\circ \ 2.41^\circ \\ &\quad *^\circ \ * \text{ft} \ * \text{ft} \ 20,000\text{ft}]^T \end{aligned} \quad (48)$$

$$\begin{aligned} u_{5B} &= [0^\circ \ 0^\circ \ 4^\circ \ 1, 195.4\text{lb}]^T \\ \gamma_{5B} &= 0^\circ, \quad \dot{\psi}_{5B} = 0^\circ/\text{s} \end{aligned}$$

Again, the above straight level flight equilibrium is consistent with the straight-level flight trim curve shown in Figure 2. At this extreme elevator jam position  $4^\circ$ , the aircraft does not have much option but to fly at a very low angle of attack with a very high total speed.



## 7 | CONCLUSION

In this paper we formulate the challenging elevator jam problem as a nonlinear multi-flight mode control problem, and these flight modes are associated with the elevator jam positions. We develop a simple effective approach to navigate the impaired aircraft toward a feasible safe level flight trim. The basic idea is simple – there exists only one single level flight trim with a specific angle of attack associated with each elevator jam position. By demanding the aircraft flight path angle to be zero, the controller and the aircraft will automatically follow the physics law to fly a level flight with the specific angle of attack. Therefore there is no need to compute this unique feasible level flight trim beforehand. This capability makes it possible to employ a simple fixed linear controller to solve this special nonlinear multi-flight mode control problem.

## ACKNOWLEDGEMENT

The research is supported in part by Army Research Laboratory under contract W911NF-15-2-0042. The second author would like to thank Dr. Mark Ilg for valuable discussions relevant to this research.

## ORCID

Po-Chun Chan  <https://orcid.org/0000-0001-7177-2671>  
Bor-Chin Chang  <https://orcid.org/0000-0001-8967-3946>

## REFERENCES

1. W. Wright, *Some aeronautical experiments – a speech to western society of engineers*, 1901. <http://www.wright-brothers.org/>
2. NTSB, *2016-preliminary-aviation-statistics.xlsx*, 2016. [https://www.nts.gov/investigations/data/Pages/aviation\\_stats.aspx](https://www.nts.gov/investigations/data/Pages/aviation_stats.aspx)
3. CM Belcastro and JV Foster, *Aircraft loss-of-control accident analysis*, Proceedings of AIAA Guidance, Navigation and Control Conference, Toronto, Canada, 2010, pp. 8004–8044.
4. AA Lambregts et al., *Airplane upsets: Old problem, new issues*, AIAA Modeling and Simulation Technologies Conference and Exhibit, Honolulu, Hawaii, 2008, pp. 6867–6878.
5. B. C. Chang et al., *Reconfigurable control of aircraft in nonlinear flight regimes*, AIAA Guidance, Navigation, and Control Conference and Exhibit, San Francisco, California, 2005, pp. 1–11.
6. H. G. Kwatny et al., *Nonlinear analysis of aircraft loss of control*, J. Guid. Control Dyn. **36** (2013), no. 1, 149–162.

7. H. G. Kwatny et al., *Aircraft accident prevention: Loss-of-control analysis*, Proceedings of the 2009 AIAA Guidance, Navigation, and Control Conference, Paper No. AIAA 2009-6256, Chicago, Illinois, 2009, pp. 6256–6269.
8. A. K. Caglayan, S. M. Allen, and K. Wehmuller, *Evaluation of a second generation reconfiguration strategy for aircraft flight control systems subjected to actuator failure surface damage*, Proceedings of the 1988 IEEE National Aerospace and Electronics Conference, Dayton, Ohio, 1988, pp. 520–529.
9. Z. Gao and P. J. Antsaklis, *Stability of the pseudo-inverse method for reconfigurable control systems*, Int. J. Control **53** (1991), no. 3, 717–729.
10. K. S. Rattan, *Evaluation of control mixer concept for reconfiguration of flight control system*, Proceedings of the 1985 IEEE National Aerospace And Electronics Conference, Dayton, Ohio, 1985, pp. 560–569.
11. Z. Yang and M. Blanke, *The robust control mixer module method for control reconfiguration*, Proceedings of the 2000 American Control Conference, Chicago, Illinois, 2000, pp. 3407–3411.
12. F. Ahmed-zaid et al., *Accommodation of failures in the f-16 aircraft using adaptive control*, IEEE Control Syst. Mag. **11** (1991), no. 1, 73–78.
13. M. Bodson and J. E. Groszkiewicz, *Multivariable adaptive algorithms for reconfigurable flight control*, IEEE Trans. Control Syst. Technol. **5** (1997), no. 2, 217–229.
14. J. D. Boskovic and R. K. Mehra, *Stable multiple model adaptive flight control for accommodation of a large class of control effector failures*, Proceedings of the 1999 American Control Conference, San Diego, 1999, pp. 1920–1924.
15. X. Tang, G. Tao, and S. M. Joshi, *Adaptive-actuator-failure-compensation-for-nonlinear-mimo-systems-with-an-aircraft-control-application*, Automatica **43** (2007), 1869–1883.
16. G. Tao, S. M. Joshi, and X. Ma, *Adaptive state feedback and tracking control of systems with actuator failures*, IEEE Trans. Autom. Control **46** (2001), no. 1, 78–95.
17. Yuanyuan Zhang, Jinkun Liu, and Wei He, *Adaptive fault-tolerant control for a nonlinear flexible aircraft wing system*, Asian J. Control **21** (2019), no. 5, 1–12.
18. G. Chowdhary et al., *Guidance and control of airplanes under actuator failures and severe structural damage*, AIAA J. Guid. Contr. Dyn. **36** (2013), no. 4, 1093–1104.
19. H. Shr-Shiung et al., *Robust nonlinear controller design for a longitudinal flight control problem*, Asian J. Control **2** (2000), no. 2, 111–121.
20. M. Lungu and R. Lungu, *Autonomous adaptive control system for airplane landing*, Asian J. Control **21** (2019), no. 4, 1–14.
21. F. Mora-Camino, S. S. Cunha, and A. Doncescu, *Aircraft flight management with actuator major failure*, 2011 Chinese Control and Decision Conference (CCDC), Mianyang, China, 2011, pp. 4311–4316.
22. D. P. Looze et al., *Nasa Contractor Report 172489: Automatic design procedures for restructurable aircraft control*, Alphatech, Inc. 2 Burlington Executive Center 111 Middlesex Turnpike Burlington, MA 01803, 1985.
23. J. L. Weiss and J. Y. Hsu, *Nasa Contractor Report 178305: Integrated restructurable flight control system demonstration results*, 1987.
24. G. Bajpai, B. C. Chang, and H. G. Kwatny, *Design of fault-tolerant systems for actuator failures in nonlinear systems*, Proceedings of the 2002 American Control Conference, Anchorage, AK, USA, 2002, pp. 3618–3623.
25. J. J. Burken et al., *Two reconfigurable flight-control design methods: Robust servomechanism and control allocation*, AIAA J. Guid. Contr. Dyn. **24** (2001), no. 3, 482–493. <https://doi.org/10.2514/2.476963>
26. B. C. Chang, G. Bajpai, and H. G. Kwatny, *A regulator design to address actuator failures*, Vol. 2, Orlando, Florida, 2001, pp. 1454–1459.
27. C. S. Buttrill, P. Douglas Arbuckle, and K. D. Hoffer, *Simulation model of a twin-tail, high performance airplane*. NASA Technical Memorandum 107601. NASA. United States, 1992.
28. A. Chakraborty, P. Seiler, and G. J. Balas, *Susceptibility of f/a-18 flight controllers to the falling-leaf mode Linear analysis*, J. Guid. Control Dyn. **34** (2011), no. 1, 57–72.
29. B. C. Chang et al., *Aircraft trim recovery from highly nonlinear upset conditions, aiaa2016-0880*, Proceedings of the 2016 AIAA Guidance, Navigation, and Control Conference, SciTech Forum, San Diego, California, 2016, pp. 1–19.
30. Bruce A Francis and W Murray Wonham, *The internal model principle of control theory*, Automatica **12** (1976), no. 5, 457–465.
31. J. Huang, *Nonlinear output regulation: Theory and applications*, SIAM, Philadelphia, 2004.
32. A. Isidori, L. Marconi, and A. Serrani, *Robust autonomous guidance: An internal model approach*, Springer Science & Business Media, Springer-Verlag London, 2003.
33. H. G. Kwatny and K. C. Kalnitsky, *On alternative methodologies for the design of robust linear multivariable regulators*, IEEE Trans. Autom. Control **AC-23** (1978), no. 5, 930–191.
34. B. L. Stevens, F. L. Lewis, and E. N. Johnson, *Aircraft control and simulation: Dynamics, controls design, and autonomous systems*, Wiley, Hoboken, New Jersey, 2016.

## AUTHOR BIOGRAPHIES



**Po-Chun Chang** received his Ph.D. in mechanical engineering from Drexel University, Philadelphia, Pennsylvania in 2018. He currently is an assistant professor in the

Department of Mechanical and Aerospace Engineering, Chung Cheng Institute of Technology in Taiwan. His research interests include robust tracking/regulation control, nonlinear control issues arising from actuator saturation, and automatic accommodation control of systems in loss-of-control conditions.



**Bor-Chin Chang** received his B.S. degree in control engineering from Chiao-Tong University in Hsin-Chu, Taiwan, M.S. degree in electrical engineering from Taiwan University in

Taipei, Taiwan, and Ph.D. in electric engineering from Rice University in Houston, Texas, in



1983. Between 1983 and 1987, he was with Bradley University in Peoria, Illinois, and since 1987 he has been with Drexel University, Philadelphia, Pennsylvania, where he currently is a professor in mechanical engineering. He was one of the contributors to the development of H-infinity control theory in the early 1980s, and a corecipient with Dr. J. B. Pearson of the *IEEE Transactions on Automatic Control* Best Paper Award in 1985 for their contribution in optimal disturbance reduction in linear multivariable systems. His current research interests include control of nonlinear systems with uncertainties, controller reconfiguration for actuator/sensor failures, real-time embedded microprocessor control, loss-of-control prevention and upset recovery for aircraft, control of flying munitions, and so on. He was an Associate Editor of the ASME Journal of Dynamic Systems, Measurement, and Control. He has been involved in funded research projects sponsored by NSF, AFOSR, Air Force Research Laboratory, NASA Langley Research Center, Army Research Laboratory, the Boeing Company, Association of Iron and Steel Engineers, Ben Franklin Partnership Program of the Commonwealth of Pennsylvania, and so on.



**Mevlut Bayram** received his B.S degree in mechanical engineering from Istanbul University in 2009 and M.S degree in mechanical engineering from Drexel University in 2013. He

is currently a Ph.D. candidate in the Department of Mechanical Engineering, Drexel University, Philadelphia, Pennsylvania, U.S.A. His research interests include aircraft flight dynamics and control and automatic reconfigured control of systems with actuator failures.



**Harry G. Kwatny** received his B.SME degree from Drexel Institute of Technology in 1961, an SM degree in aeronautics and astronautics from MIT in 1962, and a Ph.D. in electrical engineering from the University of Pennsylvania in 1967. Currently, he is the S. Herbert Raynes

Professor of Mechanical Engineering at Drexel University. He is a Life Fellow of the IEEE. Professor Kwatny's research interests include modeling, analysis and control of nonlinear, parameter-dependent systems with applications to electric generating

plants, power systems, and aircraft. His recent work has been focused on the control of impaired systems, particularly aircraft and power systems, as well as symbolic computing. He has been an Associate Editor of the *IEEE Transactions of Automatic Control* and the IFAC journal *Automatica*. He was founding Chairman of the IEEE Automatic Control Society Technical Committee on Energy and Power Systems and a member of the IFAC Committee on Power Plants and Power Systems.



**Christine M. Belcastro** received her B.Sc. in electrical engineering in May 1980, and M.Eng. in May 1986, both from Old Dominion University in Norfolk, Virginia. She received

her Ph.D. in electrical engineering in December 1994 from Drexel University in Philadelphia, Pennsylvania. She was a research engineer at the Langley Research Center of the National Aeronautics and Space Administration (NASA) for nearly 40 years as a Senior Research Engineer in the Dynamic Systems and Control Branch (DSCB). Her research interests include resilient aircraft control for multiple hazards mitigation, vehicle upset prevention and recovery, real-time aircraft flight safety assessment and assurance, autonomous and semi-autonomous vehicle systems for safety-critical applications, multidisciplinary modeling of vehicle dynamics under highly nonlinear and adverse conditions, analysis of uncertain nonlinear systems under adverse conditions, and the validation of complex integrated systems that provide real-time prediction, detection, identification, and mitigation of hazardous conditions and their implications for flight critical aircraft applications. Dr. Belcastro received the NASA Exceptional Service Medal in 2011, and was awarded the NASA Distinguished Service Medal in 2018. She retired in January 2019, and continues research as a Distinguished Research Associate at NASA Langley.

**How to cite this article:** Chan P-C, Chang B-C, Bayram M, Kwatny H, Belcastro CM. Robust tracking control of an aircraft with critical actuator jam failures. *Asian J Control*. 2020;22: 2254–2272. <https://doi.org/10.1002/asjc.2280>

## APPENDIX

### A.1 | Solution existence of Equations (24) & (38)

#### A.1.1 | Solve Equation (24) for $W, U, E$

$$AW + BU = 0 \quad \dots \quad (1)$$

$$UE - F_1WE - F_2 = 0 \quad \dots \quad (2)$$

$$C_1W + D_{11} = 0 \quad \dots \quad (3)$$

(1) \*  $E - B$  \* (2) will lead to a unique solution for  $WE = (A + BF_1)^{-1}(-BF_2)$  since  $A + BF_1$  has all its eigenvalues in the strictly left half of the complex plane and therefore is nonsingular. Multiply  $E$  to Equation (3) will lead to  $E = -D_{11}^{-1}C_1WE$ . Then from Equation (2) we have  $U = (F_1WE + F_2)E^{-1}$ .

#### A.1.2 | Solve Equation (38) for $W_{J1}, W_{J2}, U_{J1}, U_{J2}, E_J$

$$A [W_{J1} \ W_{J2}] + [B_e \ 0] + B_T [U_{J1} \ U_{J2}] = 0$$

$$C_1 [W_{J1} \ W_{J2}] + [0 \ D_{11}] = 0$$

$$U_{J2}E_J - F_1W_{J2}E_J - F_2 = 0$$

These equations can be decomposed to five equations,

$$AW_{J1} + B_T U_{J1} = -B_e \dots \quad (1)$$

$$C_1 W_{J1} = 0 \quad \dots \quad (2)$$

$$AW_{J2} + B_T U_{J2} = 0 \quad \dots \quad (3)$$

$$C_1 W_{J2} + D_{11} = 0 \quad \dots \quad (4)$$

$$U_{J2}E_J - F_1W_{J2}E_J - F_2 = 0 \quad \dots \quad (5)$$

Rewrite Equations (1) & (2) into a matrix form:

$$\begin{bmatrix} A & B_T \\ C_1 & 0 \end{bmatrix} \begin{bmatrix} W_{J1} \\ U_{J1} \end{bmatrix} = \begin{bmatrix} -B_e \\ 0 \end{bmatrix}$$

Note that  $-C_1(sI - A)^{-1}B_T$  is the transfer function from the thrust control  $\delta_T$  to the flight path angle  $\gamma = \theta - \alpha$ . Since the transfer function has no zero at  $s = 0$ , the matrix on the left of the matrix equation is nonsingular and hence there exists a unique solution for  $[W_{J1} \ U_{J1}]^T$ .

Now we will show solution existence of Equations (3), (4), (5) for  $W_{J2}, U_{J2}, E_J$ . (3) \*  $E_J - B_T$  \* (5) will lead to a unique solution for  $W_{J2}E_J = (A + B_T F_1)^{-1}(-B_T F_2)$  since  $A + B_T F_1$  has all its eigenvalues in the strictly left half of the complex plane and therefore is nonsingular. Multiply  $E_J$  to Equation (4) will lead to  $E_J = -D_{11}^{-1}C_1 W_{J2}E_J$ . Then from Equation (5) we have  $U_{J2} = (F_1 W_{J2}E_J + F_2)E_J^{-1}$ .

### A.2 | Stability analysis of the reconfigured robust tracking control system

The best chance for an impaired aircraft to survive is to first recover to a level straight flight and then maneuver to a safe landing. There is only one level flight trim available for each jam position. The proposed control system is designed to guide the aircraft to achieve zero flight path angle that will automatically lead to the only available level flight trim. However, for the proposed approach to work, the closed-loop system is required to be stable at anywhere in the operable elevator jam range.

To investigate the stability of the closed-loop system at anywhere in the operable elevator jam range  $-24^\circ < \delta_e < 5^\circ$ , the destination level flight trim  $(\hat{x}_D, \hat{u}_D)$  and its associated linearized model:  $\dot{\hat{x}}_D = A_D \hat{x}_D + B_D \hat{u}_D$  will be employed to represent any possible level flight trim and trimmed model corresponding to any elevator jam within the operable range. When an elevator jam occurs, the real aircraft or the untrimmed flight dynamics model will operate at the vicinity of the trim  $(\hat{x}_D, \hat{u}_D)$  and the local closed-loop system stability and performance can be evaluated based on the trimmed linearized model  $\dot{\hat{x}}_D = A_D \hat{x}_D + B_D \hat{u}_D$ . As shown on the righthand side of Figure A1, the untrimmed nonlinear model is replaced by the destination trimmed linear model together with trim equalizers:  $\bar{u}_D = u - \hat{u}_D$ ,  $x = \bar{x}_D + \hat{x}_D$ .

Now, we will construct the state-space representation of the closed system shown in Figure A1. From the trimmed destination model, the controller parameters, and the interconnections, we have the following equations,

$$\dot{\hat{x}}_D = A_D \bar{x}_D + B_D \bar{u}_D,$$

$$\dot{\hat{x}}_a = -C_1 \bar{x}_N$$

$$\bar{u}_D = \bar{u}_N + \hat{u}_N - \hat{u}_D, \quad \bar{x}_N = \bar{x}_D + \hat{x}_D - \hat{x}_N$$

$$\bar{\delta}_T = F_1(\bar{x}_N - W_J \rho) + U_J \rho$$

where  $B_D = [B_{De} \ B_{DT}]$

$$W_J = [W_{J1} \ W_{J2}], \quad U_J = [U_{J1} \ U_{J2}]$$

$$\bar{u}_N = \begin{bmatrix} \bar{\delta}_e \\ \bar{\delta}_T \end{bmatrix}, \quad \rho = \begin{bmatrix} \bar{\delta}_e \\ E_J \bar{x}_T \end{bmatrix}$$

Combining the above equations and the fact  $F_2 = (U_{J2} - F_1 W_{J2})E_J$  from Equation (38), we have the following

$$\begin{aligned} \dot{\hat{x}}_D &= A_D \bar{x}_D + B_{DT}(F_1 \bar{x}_D + F_2 \bar{x}_a) + \text{s.s. terms} \\ \dot{\hat{x}}_a &= -C_1 \bar{x}_D + \text{s.s. terms} \end{aligned}$$

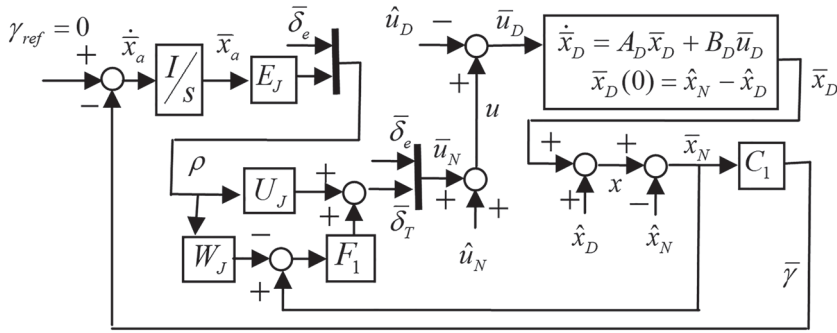


**FIGURE A1** Stability analysis of the reconfigured controller

The sum of the s.s. constant terms in each equation has to be zero unless the early trim computations were not correct. In that case, the trim values need to be revised, but the dynamic equations still remain the same. Hence, the state-space representation of the closed-loop system in matrix form at Trim  $(\hat{x}_D, \hat{u}_D)$  is

$$\begin{bmatrix} \dot{\bar{x}}_D \\ \dot{\bar{x}}_a \end{bmatrix} = \begin{bmatrix} A_D + B_{DT}F_1 & B_{DT}F_2 \\ -C_1 & 0 \end{bmatrix} \begin{bmatrix} \bar{x}_D \\ \bar{x}_a \end{bmatrix} \quad (A1)$$

The closed-loop system consisting of the proposed fixed robust tracking/regulation controller and the trimmed plant model of the impaired model  $\dot{\bar{x}}_D = A_D\bar{x}_D + B_D\bar{u}_D$  is stable (capable of converging to the level flight trim  $(\hat{x}_D, \hat{u}_D)$ ) if and only if the matrix in Equation (49) has all its eigenvalues in the strictly left half of the complex plane. We have tested two extreme cases: elevator jammed at  $-23^\circ$  and  $4^\circ$ , and many other jam positions in between. All of them are stable.